



Article

Computational Study of the Curvature-Promoted Anchoring of Transition Metals for Water Splitting

Weiwei Liu ^{1,†}, Youchao Kong ^{1,†}, Bo Wang ², Xiaoshuang Li ^{2,*}, Pengfei Liu ³, Alain R. Puente Santiago ⁴ and Tianwei He ^{5,*}

¹ Department of Physics and Electronic Engineering, Yancheng Teachers University, Yancheng 224002, China; liuww@yctu.edu.cn (W.L.); yb87816@connect.um.edu.mo (Y.K.)

² School of Applied Physics and Materials, Wuyi University, Jiangmen 529020, China; wangbo312@mails.ucas.ac.cn

³ Spallation Neutron Source Science Center, Institute of High Energy Physics, Chinese Academy of Sciences, Dongguan 523803, China; pfliu@ihep.ac.cn

⁴ Department of Chemistry and Biochemistry, University of Texas at El Paso, 500 W. University Avenue, El Paso, TX 79968, USA; arpuentesan@utep.edu

⁵ Fritz-Haber-Institute der Max-Planck-Gesellschaft, Faradayweg, 4-6, 14195 Berlin, Germany

* Correspondence: lixiaoshuang12@mails.ucas.ac.cn (X.L.); the@fhi-berlin.mpg.de (T.H.)

† These authors contributed equally to this work.

Abstract: Generating clean and sustainable hydrogen from water splitting processes represent a practical alternative to solve the energy crisis. Ultrathin two-dimensional materials exhibit attractive properties as catalysts for hydrogen production owing to their large surface-to-volume ratios and effective chemisorption sites. However, the catalytically inactive surfaces of the transition metal dichalcogenides (TMD) possess merely small areas of active chemical sites on the edge, thus decreasing their possibilities for practical applications. Here, we propose a new class of out-of-plane deformed TMD (cTMD) monolayer to anchor transition metal atoms for the activation of the inert surface. The calculated adsorption energy of metals (e.g., Pt) on curved MoS₂ (cMoS₂) can be greatly decreased by 72% via adding external compressions, compared to the basal plane. The enlarged diffusion barrier energy indicates that cMoS₂ with an enhanced fixation of metals could be a potential candidate as a single atom catalyst (SAC). We made a well-rounded assessment of the hydrogen evolution reaction (HER) and the oxygen evolution reaction (OER), which are two key processes in water splitting. The optimized Gibbs free energy of 0.02 for HER and low overpotential of 0.40 V for OER can be achieved when the proper compression and supported metals are selected. Our computational results provide inspiration and guidance towards the experimental design of TMD-based SACs.

Keywords: 2D materials; transition metal dichalcogenides; strain engineering; single atom catalyst; water splitting



Citation: Liu, W.; Kong, Y.; Wang, B.; Li, X.; Liu, P.; Santiago, A.R.P.; He, T. Computational Study of the Curvature-Promoted Anchoring of Transition Metals for Water Splitting. *Nanomaterials* **2021**, *11*, 3173. <https://doi.org/10.3390/nano11123173>

Academic Editors: Filippo Giannazzo, Ivan Shteplyuk and Maurizio Casarin

Received: 15 October 2021

Accepted: 20 November 2021

Published: 23 November 2021

Publisher's Note: MDPI stays neutral with regard to jurisdictional claims in published maps and institutional affiliations.



Copyright: © 2021 by the authors. Licensee MDPI, Basel, Switzerland. This article is an open access article distributed under the terms and conditions of the Creative Commons Attribution (CC BY) license (<https://creativecommons.org/licenses/by/4.0/>).

1. Introduction

Hydrogen gas is considered the most plausible alternative to solve the energy crisis due to its green products, high heat of combustion, and sustainable properties [1–3]. Generally, electrolytic water is believed to be a clean and simple way to generate hydrogen compared with many other methods. Proper catalysts are usually used to speed this process. The selection of traditional catalysts focuses on noble metals (like bulk Pt), for their high stability, chemical activity and selectivity, and even inter-atomic cooperation [4–6]. But the low rate of exposed active sites, high cost, and limited storage create obstacles for the widespread application of traditional catalysts.

Mono- or few-layer two-dimensional (2D) materials, with plenty of exposed chemisorption sites, easy, low-cost fabrication, and high conductivity show great potential as potential candidates to replace the traditional catalysts for water splitting [7–10]. Transition metal dichalcogenides have aroused attention among 2D materials due to their wide range of

bandgaps, strong chemical stability, and sandwich structure X–M–X since the first reported HER with MoS₂ in 2005 [11]. At that time, only TMD edges were believed to act as effective sites for catalytic processes, because the bond-free surface was inert. But the exposed sites on edges are much less than that on the surface. Hence, kinds of methods are proposed to activate the surface, such as introducing strain and defects, as well as tuning phase and heterostructure construction [12–15]. These proposed methods can promote the catalytic performance of 2D materials to some extent, but low efficiency on a per atom basis still needs to be tackled [11,16].

The atomic efficiency and low unsaturated active sites quickly caught the attention of the catalysis community since the concept of single atom catalysts (SACs) was launched in 2011 [16]. Dispersing or anchoring metal atoms/clusters on TMD thin layers greatly improved the catalytic ability of TMD-based SACs [17,18]. However, the widely adopted doping and adsorption for anchoring single atoms on graphene cannot work well in a TMD system. The formation energy of doping in MoS₂ is generally over 1.5 eV, and adsorption energy is much larger than that of doping on its basal plane, due to the weak adsorption of the S atom layer [14,19–24]. For example, Deng et al. systemically studied the possible pathways towards Pt anchoring on the surface of MoS₂, that is, the doping and adsorption of Pt atoms to promote electrolytic activity [24]. They proved that the formation energy (E_f) of Pt doping is much lower than that of Pt adsorption on the MoS₂ because it was hard to realize 3S-Pt structure in basal plane. That is why, until now, most efforts focus on the doping manner rather than adsorption (generally $E_f > 2$ eV in calculations) to promote the catalyst performance of TMD for water splitting. We also noticed that the successful realization of 3N- or 4N- Metal structure in graphene could promote the fixation of single atoms to facilitate HER, oxygen reduction reaction (ORR), and oxygen evolution reaction (OER) [25–28]. Therefore, it is necessary to figure out a suitable method to both promote the E_f and the fixation of single atoms on TMD thin layers.

Hence, we proposed a unique structure of MoS₂ monolayers to support transition metals with the combination of strain engineering and transition metals' decoration. We chose noble metal Pt and non-noble metal Fe for the assessment in our work. To evaluate the performance of metals on cMoS₂, the adsorption energy E_{ads} and diffusion barrier were calculated as a function of compressions. The great reduction (72% Max) of E_{ads} at large curvatures indicates the more possible formation of M@cMoS₂ than that on basal plane. The single atom would experience a strong fixation as the compression increases, due to the enlarged diffusion barrier up to three-fold of basal plane. We also find that E_{ads} would be further decreased under charging the situation with $1e^-$ or $2e^-$. The binding energy (E_b) of H-Fe@cMoS₂ and H-Pt@cMoS₂ is clearly affected by curvatures. The strongest binding was achieved at a curvature of 4% for Pt@cMoS₂ and 16% for Fe@cMoS₂. Correspondingly, the optimized Gibbs free energy values were -0.02 eV at 16% for Fe@cMoS₂ and 0.03 eV at 4% for Pt@cMoS₂. The HER performance could be further improved with charging one or two electrons. We also demonstrate that the large dissociation barrier of H₂O in alkaline solution resulted in a slow reaction rate of HER of the M@cMoS₂ in alkaline environment. At last, the OER performances of Pt@cMoS₂ and Fe@cMoS₂ were evaluated at different curvatures. The overpotential of 16%-Pt@cMoS₂ could be comparable to basal one but has much lower thermal energy for O₂ desorption. The promoted HER and OER of Pt or Fe anchored on MoS₂ would be expanded to other cTMDs and transition metals. The computational results pave the way towards the development of very efficient cTMD-based water splitting electrocatalysts.

2. Computational Methods

All the optimization and energy calculations are carried out with density-functional theory (DFT) to investigate the effect of surface curvature on the catalytic performance of cMoS₂. The Perdew-Burke-Eznerhof generalized gradient approximation (PBE-GGA) [29] is used for the analysis of exchange and correlation potential. The projector augmented wave (PAW) method in the Vienna ab initio simulation package (VASP) is employed in

this work [30,31]. The integration of the first Brillouin zone is carried out with the Gamma scheme of k point sampling. The used supercell is about $33 \text{ \AA} \times 10 \text{ \AA} \times 20 \text{ \AA}$ ($6\sqrt{3} \times 3 \times 1$ unit cells). A vacuum region of $\geq 15 \text{ \AA}$ is applied along the z axis to avoid the interaction between adjacent interlayers. All the calculation uses $5 \times 10^{-6} \text{ eV/atom}$ as the total energy convergence condition and 0.04 eV/\AA as the maximum force convergence criteria. All the parameters are carefully tested before further calculations. Spin-polarization is considered in our calculation and the cutoff energy is set to 500 eV. For the evaluation of the kinetic analysis, we adopt the climbing image nudged elastic band (CINEB) method to figure out the diffusion energy barrier of metal atoms on cMoS₂ and water dissociation of H₂O molecular. The model construction of curved MoS₂ monolayers is similar to our previous study [32].

The adsorption energy of metals on cMoS₂ is calculated as:

$$\Delta E_{\text{abs}} = E(\text{cMoS}_2 + \text{M}) - E(\text{cMoS}_2) - E(\text{M})$$

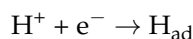
where, the $E(\text{cMoS}_2 + \text{M})$, $E(\text{cMoS}_2)$ and $E(\text{M})$ represent the total energy of monolayer curved MoS₂ with one adsorbed metal atom, the pure curved MoS₂ and the metal, respectively. Since the calculation of $E(\text{M})$ is not unified in current research, we prefer to use the calculation method, that is, the energy of bulk metal divided by the number of metal atoms. The smaller the adsorption energy, the more stable the TMs would be on the curved structures.

The binding energy of bond H-M is calculated:

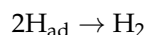
$$\Delta E_{\text{b}} = E(\text{M@cMoS}_2) + 1/2E(\text{H}_2) - E(\text{M@cMoS}_2 + \text{H})$$

where, $E(\text{M@cMoS}_2 + \text{H})$ stands for the energy of one H atom adsorbed on the metal site. $E(\text{M@cMoS}_2)$ is defined as the energy of one metal atom anchored at the center site of the crest of cMoS₂. $E(\text{H}_2)$ describes the total energy of the H₂ molecule in its gas phase. The large binding energy indicates the strong adsorption capacity of the active site for hydrogen.

The process of hydrogen evolution reaction is considered in acidic solution [2,3,33]. The first step is that a proton from the solution adsorbs on the slab and becomes an intermediate adsorbed hydrogen atom H_{ad}.



The adsorbed H atoms then combine into a hydrogen molecule.



Therefore, it is a simple calculation of the Gibbs free energy in acidic solution through the computational hydrogen electrode (CHE) method [34],

$$\Delta E_{\text{H}} = E(\text{M@cMoS}_2 + \text{H}) - E(\text{M@cMoS}_2) - 1/2E(\text{H}_2)$$

$$\Delta G_{\text{H}} = \Delta E_{\text{H}} + \Delta E_{\text{zpe}} - T\Delta S_{\text{H}}$$

where $E(\text{cMoS}_2 + \text{H})$ and $E(\text{cMoS}_2)$ represent the total energies of cMoS₂ with and without one adsorbed H, respectively. ΔE_{zpe} is the difference in zero-point energies between the adsorbed H and H in the gas phase of hydrogen molecules. $\Delta E_{\text{zpe}} - T\Delta S_{\text{H}}$ is calculated to be 0.24 eV [34].

3. Results and Discussion

3.1. Anchoring-Activity of Metal on cMoS₂

Our previous study indicated that the curved MoS could promote the surface activation due to the low adsorption energy of H atoms, but the optimized Gibbs free energy of 1.25 eV is still high for practical applications [32]. The active surface of cMoS₂ at large curvatures and the theoretically 100% efficacy of SACs catalysts could be combined to fabricate highly active catalysts. Hence, we chose noble metal (Pt) and non-noble metal (Fe)

atoms to evaluate the possible adsorption of single atoms in our unique curved structures. Figure 1 shows the schematic diagram of the possible adsorption sites of metals at the crest of $c\text{MoS}_2$, top Mo site (TM) and the center site (Hc) of honeycomb. The increasing curvature leads to a dramatic structure change along the armchair direction (Tables S1 and S2). For S-Fe (S-Pt), the a_1 is changed from 2.10 Å (2.35 Å) to 2.59 Å (3.28 Å), but the a_2 and a_3 show a limited increase, from 2.010 Å (2.35 Å) to 2.27 Å (2.38 Å). Then, the enlarged space allows metal atoms to close the inner site of Mo, which can be proved by the decreasing distance (b_1) of Fe-Mo (Pt-Mo). The b_1 changes from 2.94 Å (3.54 Å) to 2.4 Å (2.76 Å). We also noticed that even though the $\theta_{\text{S-Mo-S}}$ are still increasing, the b_1 keeps almost static after $\delta = 8\%$, which could be attributed to the repel effect between metal atoms.

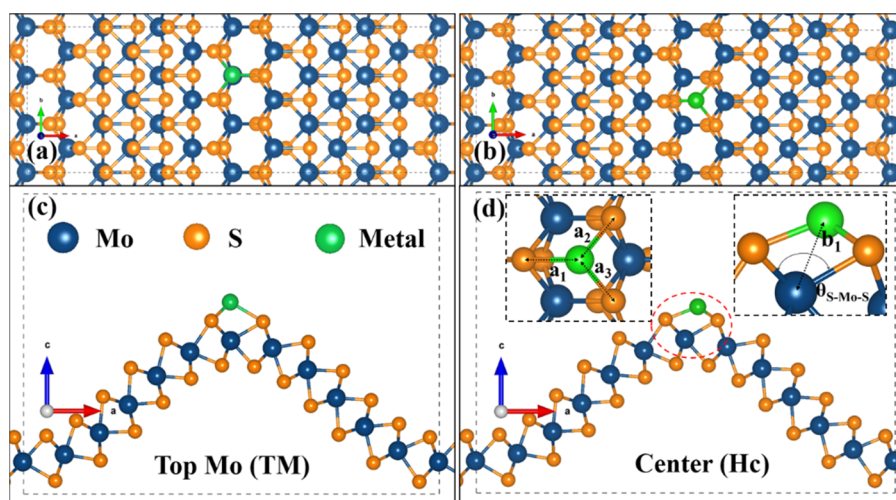


Figure 1. Representative configuration of the metal atom adsorbed on the crest of $c\text{MoS}_2$. (a,b) are the top view of the TM site and Hc site; (c,d) are the corresponding side views.

The adsorption energy of metal on TM and Hc are clearly affected with the change of curvature (Figure 2). The E_{abs} of Pt on the basal plane (0%) of MoS_2 is around 3.2 eV at Hc site and 2.6 eV at TM site, which is in agreement with previous studies [24]. As the compression increases, E_{abs} gradually reduces for Fe and Pt, but with different degrees. The Pt and Fe atoms prefer the Hc sites at larger curvatures ($\delta \geq 12\%$) rather than the TM site due to the low calculated E_{abs} at Hc sites. When the compression gets to 20%, the E_{abs} at the Hc site could be much lower to 0.9 eV (1.2 eV) with nearly 72% (49%) decrement for Pt (Fe). Remarkably, we found that E_{abs} at TM sites show a divergence between Pt and Fe when $\delta \geq 8\%$, that is, E_{abs} of Fe, keeps almost unchanged while Pt shows a continuous decrease. Our calculation found that Top S (tS) is the most impossible to adsorb metal due to the much larger adsorption energy than that of the other two sites, which is consistent with previous reports [24]. Besides, the curvature has no positive effect on the Fe or Pt adsorption activity at tS on $c\text{MoS}_2$ (Figure S1).

The systems charged with one electron and two electrons were also calculated for simulating the real situation in experiments. Figure 2b shows that the trend of E_{b} at the H site is similar to the neutral situation. The increasing number of electrons into the system results in a promotion of the metal adsorption of $c\text{MoS}_2$, that is, the E_{ads} with $1e^-$ is lower than that with $2e^-$. The difference of E_{ads} between $1e^-$ and $2e^-$ is enlarged at $\delta \geq 12\%$, which would mean that the large curvature helps adsorbents attract more extra charge. The unstable structure of Pt- $c\text{MoS}_2$ is observed when $\delta > 16\%$, which would result from the weak interaction of S-Pt induced by the enlarged a_1 in a charged system (Tables S2–S4).

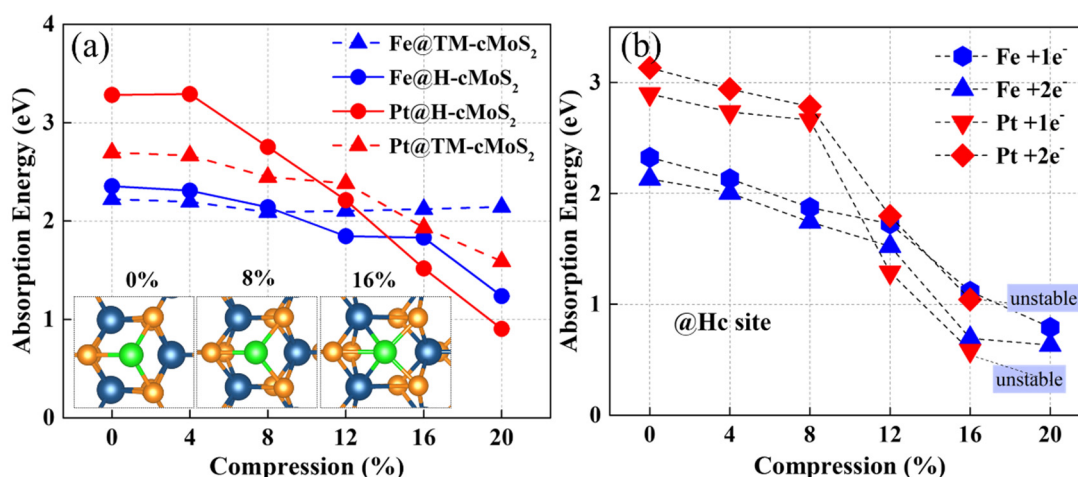


Figure 2. (a) The adsorption energy of metal atoms on neutral cMoS₂ as a function of compressions. The insets represent the top view of M@cMoS₂ at different compressions. (b) The adsorption energy of metal atoms on the H site of charged cMoS₂ as a function of compressions.

To dig out the relationship between the adsorption energy and the curvature of cMoS₂, the charge density difference isosurface and Bader charge transfer are calculated (Figure 3). In the sandwiched structure of MoS₂, generally, the middle layer of Mo atoms is screened by outer S atoms, which makes the adsorbate hard to interact with the Mo layer. Moreover, the saturated surface bonds of the S atom layer show a weak adsorption of most adsorbates, leading to an inert chemical activity [35]. For the basal plane (0%) MoS₂, the Pt and Fe atoms show less effect on the charge density of Mo (Figure 3a,d). As the curvature increases, the distance of Pt/Fe-Mo decreases (b_1 in Tables S1 and S2). Then, a strong interaction between Pt/Fe and Mo appears at a large compression, which is indicated by the large charge density transfer (Figure 3c,f). The calculated Bader transfer also proves the electronic redistribution. For example, the Bader charges of Fe and Pt are -0.64 eV and -0.1 eV at 0%-cMoS₂, which increase to -0.24 eV and $+0.25$ eV at 16%-cMoS₂ (Table S3). The higher charge transfer indicates a stronger interaction. In addition, the charged electrons accumulate around the adsorbates to further increase the ability of the adsorption. For example, the increasing electrons accumulate around Pt after more electrons charged into the system (Figure S2). Therefore, the more electrons accumulate around adsorbates, the stronger adsorption cMoS₂ has. Because of the strong ability to adsorb single atoms, monolayer MoS₂ with its curved deformation has the potential to act as a single-atom catalyst, which could be further proved by the AIMD simulation at room temperature (Figure S3).

Another important issue of potential SACs focuses on their stability on the surface of the slab, meaning the single atom would not diffuse arbitrarily. Hence, we calculated the diffusion barrier of Pt and Fe on the crest of MoS₂. Figure 4a shows the possible diffusion pathway for a single atom: P1 and P2. The results show that P2 is more possible than P1, because the E_b of top Mo along the P2 is lower than that of the bridge of S-Mo along P1. From Figure 4b, we can see the energy and optimized structures of three states when the Fe atom would diffuse on the surface of cMoS₂. For a basal plane, the adsorption energy of Fe is slightly different (Figure 2a). The Fe atom needs to conquer an energy barrier of 0.89 eV to arrive to the TM site. The energy of final state (FS) is a negative value, due to the lower E_{ads} at TM than that at Tc. But for Pt atoms, the large difference of E_{ads} between TM and Tc leads to a barrierless movement from Hc to TM on basal MoS₂ (Figure S4).

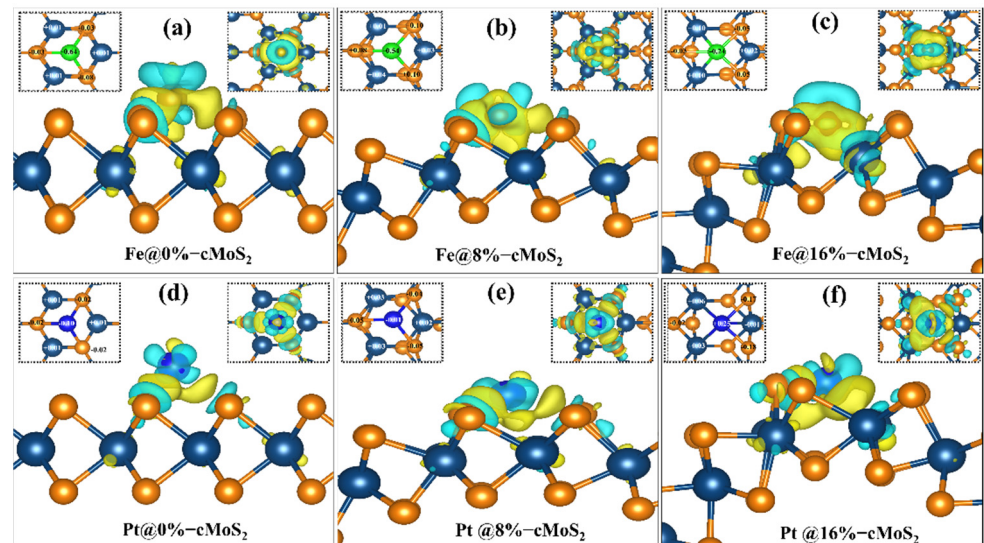


Figure 3. (a–f) The charge density difference between $cMoS_2$ and $Fe@cMoS_2$ (the upper)/ $Pt@cMoS_2$ (the lower). The yellow and blue represent the charge accumulation and dissociation. The left and right insets indicate the Bader charge change around adsorbents and the top view of charge density difference for each situation. The isosurface value is set to $0.004 e/\text{\AA}^3$.

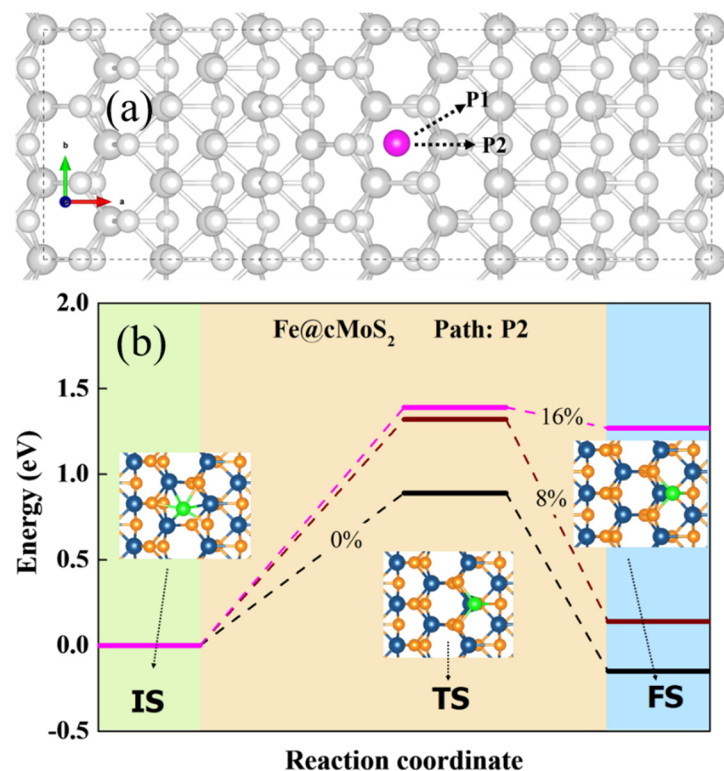


Figure 4. (a) The possible pathway of M diffusion in $cMoS_2$. (b) The diffusion coordinates of the Fe atom in $cMoS_2$ at different compressions. The inset is the corresponding top view of different states.

As the curvature enlarges, Fe and Pt have difficulty going down the curved surface due to the increasing energy of the transition state (TS) (Figure 4b and Figure S4). In comparison with basal plane, the diffusion barrier experiences 1.6-fold ($0.89 \text{ eV} \rightarrow 1.4 \text{ eV}$) and 3-fold ($0.45 \text{ eV} \rightarrow 1.5 \text{ eV}$) increments for Fe and Pt, respectively. Additionally, atoms are difficult to anchor at other sites when $\delta \geq 16\%$, since the energy of FS increases sharply from $\delta = 8\%$ to $\delta = 16\%$, which would strengthen the fixation selectivity of metals adsorbed

on cMoS₂. Overall, the curvature-promoted single-atom-anchored on cMoS₂ indicates a great potential as SACs.

3.2. Hydrogen Evolution Reaction

To evaluate the ability of water splitting based on metal-decorated cMoS₂, we first investigated the hydrogen evolution reaction based on Fe@cMoS₂ and Pt@cMoS₂. The HER reaction mechanism depends on the pH of the solution. In acid solution, a sufficient H⁺ became indeterminate of H_{ad} after getting electrons from the electrode [2]. The key issue is that the surface of catalysts provides active sites to combine two adsorbed H_{ad} into H₂ gas. Hence, we first calculate the binding energy (E_b) of an H-M bond to evaluate the adsorption of H on Pt@cMoS₂ and Fe@cMoS₂. From Figure 5a,b, the basal plane of Pt@MoS₂ is more active for the H adsorption than that of Fe@MoS₂, due to the high binding energy 0.18 eV than 0.1 eV of Fe. The positive value (Figure 5b) indicates it is an exothermic process in a Pt-based catalyst, which is in agreement with other reports [36]. The E_b is fluctuating within the range of 0.5 eV along with the increment of the compression. The E_b of H-Pt initially goes up to 0.21 eV by adding small stress, and then linearly decreases to -0.08 eV ($\delta = 12\%$), indicating a weak trend of H adsorption. A dominant improvement of binding appears at large curvatures. H-Fe shows a similar trend, but the turning point (8%) is earlier than Pt, which is attributed to the magnetic influence. All in all, we find that the strongest binding of H-Pt appears at a small compression of 4%, while that of H-Fe is larger ($\delta = 16\%$). It should be noted that the structure of M@cMoS₂ becomes unstable after one H atom absorbs on it under a large compression ($>16\%$).

We then considered the charging situation. With one extra electron, the trend of binding energy is similar to the neutral one as compression increases (Figure 5a,b), except for the H-Pt@cMoS₂ with 2e⁻ (Figure 5b). Because the extra electron leads to the shifting of the Pt adsorption position from H_c to TM and then induces a strange binding energy of H-Pt on 0%-cMoS₂. Compared with a neutral situation, charging one electron brings a stronger binding between the H atom and the Fe/Pt atom at the small curvature ($\delta \leq 8\%$), due to the much higher binding energy. For example, E_b of H-Fe is above zero with one extra electron, which means a spontaneous adsorption of the H atom. When the compression gets large, the binding energy is distinguished. The E_b with one electron is smaller than that in a neutral system for H-Fe after 16% and for H-Pt after 12%. This finding indicates the adsorption of H becomes weak, which would result in more 3d empty orbitals of metals being occupied by extra electrons, since the overlap of charge density between Mo and Fe or Pt gets larger at a high compression (Figure 3c,f). This conclusion can be further proved by the adsorption results with two electrons charging [37]. The curvature facilitates the injection of electrons to the adatoms (Fe, Pt) via the exposed Mo atom at a large compression, and then fewer empty orbitals lead to a weak adsorption.

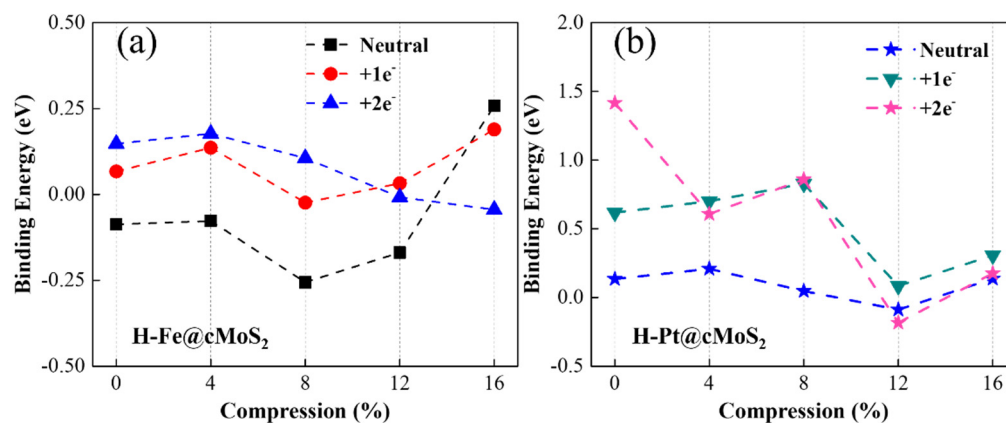


Figure 5. Binding energy of Fe@cMoS₂ (a) and Pt@cMoS₂ (b) as a function of compressions at neutral, +1e⁻ and 2e⁻ situations.

The Gibbs free energy (ΔG_H) is widely used to judge the HER performance of a catalyst. Since HER involves two steps (H adsorption and H_2 desorption), the optimized ΔG_H is equal to zero. For the specific site of unsaturated single atoms supported on $cMoS_2$, we calculate the Gibbs free energy for the first (green), second (blue), and third hydrogen atoms (red) at different curvatures (Figure 6). For $Fe@cMoS_2$ from 0% to 12%, we find that the high reaction activity appears when the second H atom is adsorbed, and the low HER activity with one H, due to the low reaction barrier at each compression (the blue line closes to 0 eV). The optimized ΔG_H of 0.03 eV is achieved at $\delta = 8\%$. But at large curvatures (16%), the high HER activity ($\Delta G = -0.02$ eV) would be achieved when $Fe@cMoS_2$ adsorbs one hydrogen, because the strong binding ($\Delta G = -0.43$ eV) of H-Fe-H needs energy for H_2 desorption with one more hydrogen adsorbed. Meanwhile, for $Pt@cMoS_2$, the strong interaction between $2H/3H$ and Pt indicates the difficult desorption of H_2 at small curvatures. Instead, the one electron is possible due to the lower reaction barrier. The optimized Gibbs free energy (0.03 eV) is located at 8%-Pt@cMoS₂. But when compression gets to 12%, the Pt with two electrons owns high activity ($\Delta G = -0.03$ eV). After 12%, Pt@cMoS₂ shows an unstable structure with one more hydrogen adsorbed. Therefore, the curved MoS₂ with metals anchored have a great potential for HER under a proper compression force.

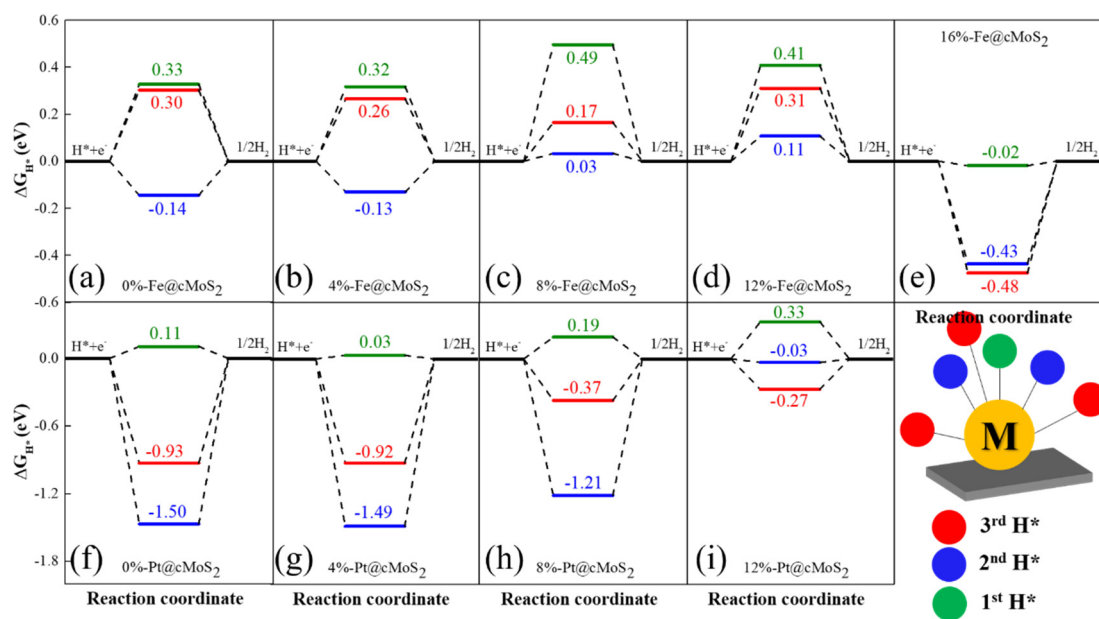


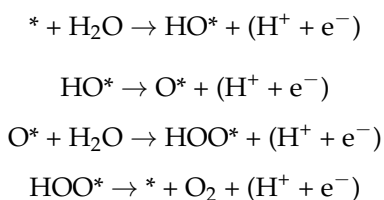
Figure 6. (a–i) The free energy diagram of $Fe@cMoS_2$ and $Pt@cMoS_2$ for hydrogen evolution reactions at different compressions. The Gibbs free energy of an ideal catalyst for the HER should be close to 0.

Additionally, the catalytic performance of $Pt@MoS_2$ and $Fe@MoS_2$ in neutral or alkaline solutions are also investigated. Different from the acid electrolyte, the proton is the minority in alkaline one. The first step is the water dissociation, in which the H_2O molecule would adsorb on an active surface and then dissociate into OH^- and H^+ [34]. The calculated dissociation barrier is larger than that of a traditional Pt/C electrode due to the weak binding between H and S atoms. All the details are discussed in the supporting information (Figures S5 and S6).

3.3. Oxygen Evolution Reaction

The oxygen evolution reaction (OER) is another key half reaction that involves four electrons transfer steps in the electrocatalytic water splitting, the same importance to HER. Therefore, a correct assessment of OER is beneficial for an in-depth understanding of the catalyst for water splitting. Up to now, the metal-based catalysts for OER mainly focus on

the edge effect and edge-supported single atoms [38–40]. For instance, Xu et al. reported a Pt anchored at the edge of MoS₂ demonstrated an ultra-low overpotential (η) of 0.46 V, which delivered a performance close to the bulk noble metal [38]. Similarly, the limited area of the edge restricted its massive application. The recent experimental results show that co-doping MoS₂ exhibited a similar result ($\eta_{\min} = 0.48$ V) to the edge MoS₂ but provided sufficient active reaction sites [41]. This provides a clear direction to the TMD-based SACs. However, the large doping energy (>2 eV, in calculation) makes doping difficult to some extent [42,43]. The above discussed adsorption promotion of metals in our system would alleviate the problem to a more possible degree. Here, we calculate the four electron transfer steps and make an assessment of OER in the M@cMoS₂. The OER is a four-electron water oxidation process, and the probable reaction mechanism steps are as follows [2,3]:



The Gibbs free energy of each step is calculated as the HER reaction in the previous part.

Figure 7a shows the optimized structure for each reaction step. The OER reaction is clearly tuned by the curvature at equilibrium hydrolysis potential (Figure 7b). We see that the enlarged curvature leads to a weak *OH adsorption of Pt@cMoS₂. The potential determining step (PDS) is *OH oxidation (Step II) at a small curvature ($\leq 8\%$), while PDS locates at the step *O \rightarrow *OOH (Step III) at $\delta = 16\%$. The reaction rate would be 0%-Pt@cMoS₂ > 16%-Pt@cMoS₂ > 8%-Pt@cMoS₂, which PDS are 0.31 eV, 0.40 eV and 1.04 eV. But the last step contains a thermal desorption of O₂ from the slab, the production of O₂ on 16%-Pt@cMoS₂ would be more than that on 0%-Pt@cMoS₂, due to the different trend between the downhill step and uphill step at Step IV for 16% and 0%, respectively. For Fe@cMoS₂, the strong binding between *O and Fe leads to an easy oxidation of *OH (Step II, Figure S7). The determining steps are all located at Step III, and are 0.93 eV, 1.01 eV, and 1.13 eV for 0%, 8%, and 16%, respectively. The effect of curvatures on the OER performance of Fe@cMoS₂ is similar to that of Pt@cMoS₂. But the much larger PDS of Fe@cMoS₂ obstacles its practical application. We also consider another pathway for *O \rightarrow *OOH. For example, the *O and *OH adsorb on the metal at the same time, but the large formation energy and physical adsorption format make the pathway impossible. It means the metal decorated-cMoS₂ has a good selectivity as an OER catalyst. Therefore, it is believed that M@cMoS₂ would be used as a potential SAC candidate for OER if the proper anchored metals and curvatures are selected.

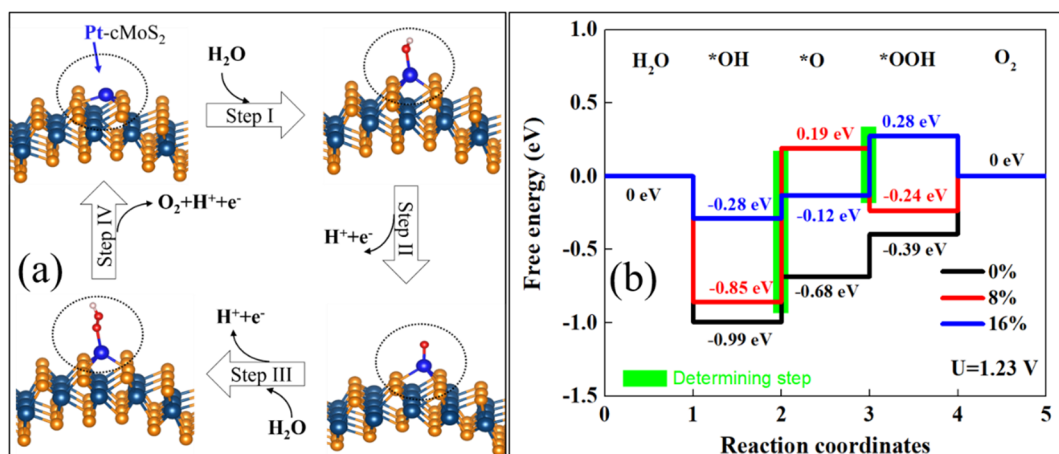


Figure 7. (a) Proposed 4e-mechanism of oxygen evolution reaction on Pt@cMoS₂. (b) Gibbs free-energy diagram for the four steps of OER on Pt@cMoS₂ at different curvatures. The green box step is the rate determining.

4. Conclusions

In summary, we have proposed an effective structure with an aim to activate the inert surface of TMD monolayers, which are believed to be activated by an edge effect or prior doping. We took the noble metal Pt and nonnoble metal Fe as examples. Compared with the basal MoS₂, the curved one demonstrated a promoted ability to hold metal atoms, especially at center sites of the honeycomb structure on the crest cMoS₂ with large curvatures. The promotion can be up to 72% for Pt@cMoS₂. Additionally, the CINEB calculation showed the diffusion barrier increased to the point that the metal atom was stable at the H site under large compressions. Moreover, we made a series of assessments of water splitting based on the single atom anchored at cMoS₂. The excellent HER appeared at 4%-cMoS₂ for Pt and at 16%-cMoS₂ for Fe, and are comparable to the traditional bulk electrode Pt/C. However, the ability of water dissociation was still inferior in our system, which indicated a limited HER performance in alkane solution. At last, the calculated OER at 16%-Pt@cMoS₂ showed a fast reaction, due to the low PDS of 0.40 eV and the downhill step of O₂ desorption compared with the basal plane at the equilibrium potential. Our calculations provide insightful explanations for the design of TMD-based SACs, suggesting that the curved-TMD represents a feasible approach to fabricate efficient SA water splitting electrocatalysts.

Supplementary Materials: The following are available online at <https://www.mdpi.com/article/10.3390/nano1123173/s1>, Figure S1: Adsorption energy of Fe and Pt atoms at top S site on neutral cMoS₂ as a function of compressions, Figure S2: Charge density difference of Pt@cMoS₂ in neutral (a,d), 1e⁻ (b,e) and 2e⁻ (c,f) situations. The isosurface value is set to 0.004 e/Å³, Figure S3: AIMD simulation of Pt-12%cMoS₂ as a function of simulation time. The timespan is over 4 ps, Figure S4: Diffusion coordinates of Pt atom in cMoS₂ at different compressions, Figure S5: Optimized structures for the initial (IS, leftmost panels), transition (TS, center panels), and final (FS, rightmost panels) states of the most favorable path for the H₂O → OH⁻ + H⁺ reaction on Fe@cMoS₂, Figure S6: Reaction coordinate of water dissociation of Fe@cMoS₂ at δ = 16% and the comparison with Pt bulk, Figure S7: Gibbs free-energy diagram for the four steps of OER on Fe@cMoS₂ at different curvatures. The green box step is the rate determining, Table S1: Structure parameters of cMoS₂ absorbed Fe atom as compressions increases, Table S2: Structure parameters of cMoS₂ absorbed Pt atom as compressions increases, Table S3: Bader charge of Fe@cMoS₂ at different compressions, Table S4: Bader charge of Pt@cMoS₂ at different compressions.

Author Contributions: Conceptualization, W.L. and Y.K.; methodology, Y.K.; software, P.L.; validation, B.W. and T.H.; formal analysis, Y.K.; investigation, W.L. and Y.K.; resources, X.L.; data curation, Y.K.; writing—original draft preparation, W.L.; writing—review and editing, A.R.P.S., T.H.; supervision, X.L.; funding acquisition, B.W. and X.L. All authors have read and agreed to the published version of the manuscript.

Funding: This work was supported by the National Natural Science Foundation of China (No. 61504118, 51902226, 52002288), the Natural Science Foundation of Jiangsu Province (No. BK20130423), and the National Natural Science Foundation of Guangdong Province (No.2019A1515012072), the research and development fund of Wuyi University joint Hong Kong-Macao (No. 2019WGALH04, No. 2019WGALH09).

Conflicts of Interest: The authors declare no conflict of interest.

References

1. Momirlan, M.; Veziroglu, T. Current status of hydrogen energy, *Renew. Sustain. Energy Rev.* **2002**, *6*, 141–179. [[CrossRef](#)]
2. Murthya, A.; Madhavana, J.; Muruganb, K. Recent advances in hydrogen evolution reaction catalysts on carbon/carbon-based supports in acid media. *J. Power Sources* **2018**, *398*, 9–26. [[CrossRef](#)]
3. Wu, Y.; Yao, J.; Gao, J. Interface Chemistry of Platinum-Based Materials for Electrocatalytic Hydrogen Evolution in Alkaline Conditions. In *Methods for Electrocatalysis*; Springer: Cham, Switzerland, 2020. [[CrossRef](#)]
4. Zou, X.X.; Zhang, Y. Noble metal-free hydrogen evolution catalysts for water splitting. *Chem. Soc. Rev.* **2015**, *44*, 5148–5180. [[CrossRef](#)] [[PubMed](#)]
5. Wang, J.; Xu, F.; Jin, H.; Chen, Y.; Wang, Y. Non-Noble Metal-based Carbon Composites in Hydrogen Evolution Reaction: Fundamentals to Applications. *Adv. Mater.* **2017**, *29*, 1605838. [[CrossRef](#)] [[PubMed](#)]
6. Cheng, N.; Stambula, S.; Wang, D.; Banis, M.N.; Liu, J.; Riese, A.; Xiao, B.; Li, R.; Sham, T.-K.; Liu, L.-M.; et al. Platinum single-atom and cluster catalysis of the hydrogen evolution reaction. *Nat. Commun.* **2016**, *7*, 13638. [[CrossRef](#)]
7. Voiry, D.; Yang, J.; Chhowalla, M. Recent Strategies for Improving the Catalytic Activity of 2D TMD Nanosheets Toward the Hydrogen Evolution Reaction. *Adv. Mater.* **2016**, *28*, 6197–6206. [[CrossRef](#)] [[PubMed](#)]
8. Di, J.; Yan, C.; Handoko, A.D.; Seh, Z.W.; Li, H.; Liu, Z. Ultrathin two-dimensional materials for photo- and electrocatalytic hydrogen evolution. *Mater. Today* **2018**, *21*, 749–770. [[CrossRef](#)]
9. Lu, Q.; Yu, Y.; Ma, Q.; Chen, B.; Zhang, H. 2D Transition-Metal-Dichalcogenide-Nanosheet-Based Composites for Photocatalytic and Electrocatalytic Hydrogen Evolution Reactions. *Adv. Mater.* **2016**, *28*, 1917–1933. [[CrossRef](#)] [[PubMed](#)]
10. Novoselov, K.S.; Mishchenko, A.; Carvalho, A.; Neto, A.H.C. 2D materials and van der Waals heterostructures. *Science* **2016**, *353*, aac9439. [[CrossRef](#)]
11. Hinnemann, B.; Moses, P.G.; Bonde, J.; Jørgensen, K.P.; Nielsen, J.H.; Horch, S.; Chorkendorff, I.; Nørskov, J.K. Biomimetic Hydrogen Evolution: MoS₂ Nanoparticles as Catalyst for Hydrogen Evolution. *J. Am. Chem. Soc.* **2005**, *127*, 5308–5309. [[CrossRef](#)] [[PubMed](#)]
12. Deng, D.; Novoselov, K.; Fu, Q.; Zheng, N.; Tian, N.Z.Z.; Bao, X. Catalysis with two-dimensional materials and their heterostructures. *Nat. Nanotechnol.* **2016**, *11*, 218–230. [[CrossRef](#)] [[PubMed](#)]
13. Zhang, X.; Zhang, Z.; Wu, D.; Zhang, X.; Zhao, X.; Zhou, Z. Computational Screening of 2D Materials and Rational Design of Heterojunctions for Water Splitting Photocatalysts. *Small Methods* **2018**, *2*, 1700359. [[CrossRef](#)]
14. Shi, Y.; Zhou, Y.; Yang, D.-R.; Xu, W.-X.; Wang, C.; Wang, F.-B.; Xu, J.-J.; Xia, X.-H.; Chen, H.-Y. Energy Level Engineering of MoS₂ by Transition-Metal Doping for Accelerating Hydrogen Evolution Reaction. *J. Am. Chem. Soc.* **2017**, *139*, 15479–15485. [[CrossRef](#)] [[PubMed](#)]
15. Le, D.; Rawal, T.B.; Rahman, T.S. Single-Layer MoS₂ with Sulfur Vacancies: Structure and Catalytic Application. *J. Phys. Chem. C* **2014**, *118*, 5346–5351. [[CrossRef](#)]
16. Qiao, B.; Wang, A.; Yang, X.; Allard, L.F.; Jiang, Z.; Cui, Y.; Liu, J.; Li, J.; Zhang, T. Single-atom catalysis of CO oxidation using Pt₁/FeOx. *Nat. Chem.* **2011**, *3*, 634–641. [[CrossRef](#)] [[PubMed](#)]
17. Alarawi, A.A.; Ramalingam, V.; He, J.-H. Recent advances in emerging single atom confined two-dimensional materials for water splitting applications. *Mater. Today Energy* **2019**, *11*, 1–23. [[CrossRef](#)]
18. He, T.; Zhang, C.; Du, A. Single-atom supported on graphene grain boundary as an efficient electrocatalyst for hydrogen evolution reaction. *Chem. Eng. Sci.* **2019**, *194*, 58–63. [[CrossRef](#)]
19. Ma, D.; Li, T.; Zhang, X.; He, C.; Tang, Y.; Yang, Z. Modulating electronic, magnetic and chemical properties of MoS₂ monolayer sheets by substitutional doping with transition metals. *Appl. Surf. Sci.* **2016**, *364*, 181–189. [[CrossRef](#)]
20. Saab, M.; Raybaud, P. Tuning the Magnetic Properties of MoS₂ Single Nanolayers by 3d Metals Edge Doping. *J. Phys. Chem. C* **2016**, *120*, 10691–10697. [[CrossRef](#)]
21. Zhu, Y.; Peng, W.; Li, Y.; Zhang, G.; Zhang, F.; Fan, X. Modulating the Electronic Structure of Single-Atom Catalysts on 2D Nanomaterials for Enhanced Electrocatalytic Performance. *Small Methods* **2019**, *3*, 1800438. [[CrossRef](#)]
22. Qi, K.; Yu, S.; Wang, Q.; Zhang, W.; Fan, J.; Zheng, W.; Cui, X. Decoration of the Inert Basal Plane of Defect-Rich MoS₂ with Pd Atoms for Achieving Pt-Similar HER Activity. *J. Mater. Chem. A* **2016**, *4*, 4025–4031. [[CrossRef](#)]
23. Lin, L.; Sherrell, P.; Liu, Y.; Lei, W.; Zhang, S.; Zhang, H.; Wallace, G.G.; Chen, J. Engineered 2D Transition Metal Dichalcogenides—A Vision of Viable Hydrogen Evolution Reaction Catalysis. *Adv. Energy Mater.* **2020**, *10*, 1903870. [[CrossRef](#)]
24. Deng, J.; Li, H.; Xiao, J.; Tu, Y.; Deng, D.; Yang, H.; Tian, H.; Li, J.; Ren, P.; Bao, X. Triggering the electrocatalytic hydrogen evolution activity of the inert two-dimensional MoS₂ surface via single-atom metal doping. *Energy Environ. Sci.* **2015**, *8*, 1594–1601. [[CrossRef](#)]

25. Chung, H.T.; Cullen, D.A.; Higgins, D.; Sneed, B.T.; Holby, E.F.; More, K.L.; Zelenay, P. Direct atomic-level insight into the active sites of a high-performance PGM-free ORR catalyst. *Science* **2017**, *357*, 479–484. [[CrossRef](#)]
26. Fei, H.; Dong, J.; Arellano-Jiménez, M.J.; Ye, G.; Kim, N.D.; Samuel, E.L.G.; Peng, Z.; Zhu, Z.; Qin, F.; Bao, J.; et al. Atomic cobalt on nitrogen-doped graphene for hydrogen generation. *Nat. Commun.* **2015**, *6*, 8668. [[CrossRef](#)] [[PubMed](#)]
27. He, T.; Matta, S.; Will, G.; Du, A. Transition-metal single atoms anchored on graphdiyne as high-efficiency electrocatalysts for water splitting and oxygen reduction. *Small Methods* **2019**, *3*, 1800419. [[CrossRef](#)]
28. Cheng, N.; Zhang, L.; Doyle-Davis, K.; Sun, X. Single-Atom Catalysts: From Design to Application. *Electrochem. Energy Rev.* **2019**, *2*, 539–573. [[CrossRef](#)]
29. Blöchl, P.E. Projector Augmented-wave Method. *Phys. Rev. B* **1994**, *50*, 17953. [[CrossRef](#)]
30. Kresse, G.; Furthmüller, J. Efficient iterative schemes for ab initio total-energy calculations using a plane-wave basis set. *Phys. Rev. B* **1996**, *54*, 11169. [[CrossRef](#)] [[PubMed](#)]
31. Kresse, G.; Furthmüller, J. Efficiency of ab-initio total energy calculations for metals and semiconductors using a plane-wave basis set. *Comp. Mater. Sci.* **1996**, *6*, 15–50. [[CrossRef](#)]
32. Kong, Y.; Ai, H.; Wang, W.; Xie, X.; Lo, K.H.; Wang, S.; Pan, H. Waved 2D Transition-Metal Disulfides for Nanodevices and Catalysis: A First-Principle Study. *ACS Appl. Nano Mater.* **2020**, *3*, 2804–2812. [[CrossRef](#)]
33. Laursen, A.B.; Varela, A.S.; Dionigi, F.; Fanchiu, H.; Miller, C.; Trinhammer, O.L.; Rossmeisl, J.; Dahl, S. Electrochemical Hydrogen Evolution: Sabatier’s Principle and the Volcano Plot. *J. Chem. Educ.* **2012**, *89*, 1595–1599. [[CrossRef](#)]
34. Nørskov, J.; Rossmeisl, J.; Logadottir, A.; Lindqvist, L.; Kitchin, J.R.; Bligaard, T.; Jonsson, H. Origin of the Overpotential for Oxygen Reduction at a Fuel-Cell Cathode. *J. Phys. Chem. B* **2004**, *108*, 17886–17892. [[CrossRef](#)]
35. Joshi, Y.V.; Ghosh, P.; Venkataraman, P.S.; Delgass, W.N.; Thomson, K.T. Electronic Descriptors for the Adsorption Energies of Sulfur-Containing Molecules on Co/MoS₂, Using DFT Calculations. *J. Phys. Chem. C* **2009**, *113*, 9698–9709. [[CrossRef](#)]
36. Fajín, J.L.C.; Cordeiro, M.N.D.S.; Gomes, J.R.B. Density Functional Theory Study of the Water Dissociation on Platinum Surfaces: General Trends. *J. Phys. Chem. A* **2014**, *118*, 5832–5840. [[CrossRef](#)] [[PubMed](#)]
37. Sun, Q.; Li, Z.; Searles, D.; Chen, Y.; Lu, G.; Du, A. Charge-Controlled Switchable CO₂ Capture on Boron Nitride Nanomaterials. *J. Am. Chem. Soc.* **2013**, *135*, 8246–8253. [[CrossRef](#)] [[PubMed](#)]
38. Xu, X.; Xu, H.; Cheng, D. Design of high-performance MoS₂ edge supported single-metal atom bifunctional catalysts for overall water splitting via a simple equation. *Nanoscale* **2019**, *11*, 20228–20237. [[CrossRef](#)] [[PubMed](#)]
39. Tang, B.; Yu, Z.G.; Seng, H.L.; Zhang, N.; Liu, X.; Zhang, Y.-W.; Yang, W.; Gong, H. Simultaneous edge and electronic control of MoS₂ nanosheets through Fe doping for an efficient oxygen evolution reaction. *Nanoscale* **2018**, *10*, 20113–20119. [[CrossRef](#)] [[PubMed](#)]
40. Mohanty, B.; Ghorbani-Asl, M.; Kretschmer, S.; Ghosh, A.; Guha, P.; Panda, S.K.; Jena, B.; Krasheninnikov, A.V.; Jena, B.K. MoS₂ Quantum Dots as Efficient Catalyst Materials for the Oxygen Evolution Reaction. *ACS Catal.* **2018**, *8*, 1683–1689. [[CrossRef](#)]
41. Xiong, Q.; Wang, Y.; Liu, P.F.; Zheng, L.R.; Wang, G.; Yang, H.G.; Wong, P.K.; Zhang, H.; Zhao, H. Cobalt Covalent Doping in MoS₂ to Induce Bifunctionality of Overall Water Splitting. *Adv. Mater.* **2018**, *30*, e1801450. [[CrossRef](#)]
42. Li, Q.; Zhao, X.; Deng, L.; Shi, Z.; Liu, S.; Wei, Q.; Zhang, L.; Cheng, Y.; Zhang, L.; Lu, H.; et al. Enhanced Valley Zeeman Splitting in Fe-Doped Monolayer MoS₂. *ACS Nano* **2020**, *14*, 4636–4645. [[CrossRef](#)] [[PubMed](#)]
43. Mombrú, D.; Faccio, R.; Mombrú, Á.W. Possible doping of single-layer MoS₂ with Pt: A DFT study. *Appl. Surf. Sci.* **2018**, *462*, 409–416. [[CrossRef](#)]